

Michail Michailov
(Editor)

Nanophenomena at Surfaces

Fundamentals
of Exotic Condensed Matter Properties

With 145 Figures

Springer Series in Surface Sciences ISSN 0931-5195
ISBN 978-3-642-16509-2 e-ISBN 978-3-642-16510-8
DOI 10.1007/978-3-642-16510-8
Springer Heidelberg Dordrecht London New York

© Springer-Verlag Berlin Heidelberg 2011

This work is subject to copyright. All rights are reserved, whether the whole or part of the material is concerned, specifically the rights of translation, reprinting, reuse of illustrations, recitation, broadcasting, reproduction on microfilm or in any other way, and storage in data banks. Duplication of this publication or parts thereof is permitted only under the provisions of the German Copyright Law of September 9, 1965, in its current version, and permission for use must always be obtained from Springer. Violations are liable to prosecution under the German Copyright Law.

The use of general descriptive names, registered names, trademarks, etc. in this publication does not imply, even in the absence of a specific statement, that such names are exempt from the relevant protective laws and regulations and therefore free for general use.

 Springer

Chapter 2 Multisite Interactions in Lattice-Gas Models

T.L. Einstein and R. Sathiyarayanan

Abstract For detailed applications of lattice-gas models to surface systems, multisite interactions often play at least as significant a role as interactions between pairs of adatoms that are separated by a few lattice spacings. We recall that trio (3-adatom, non-pairwise) interactions do not inevitably create phase boundary asymmetries about half coverage. We discuss a sophisticated application to an experimental system and describe refinements in extracting lattice-gas energies from calculations of total energies of several different ordered overlayers. We describe how lateral relaxations complicate matters when there is direct interaction between the adatoms, an issue that is important when examining the angular dependence of step line tensions. We discuss the connector model as an alternative viewpoint and close with a brief account of recent work on organic molecule overlayers.

2.1 Introduction

A thorough understanding and characterization of surface energetics is important for fabricating nanostructures with desired morphological features. To this end, lattice-gas models have been very successful in categorizing structural properties, energetics, and evolution of adatoms and steps on surfaces, as discussed in a variety of reviews [1–4]. They have also been applied to analogous but more complicated systems [5], such as electrochemistry [6]. The underlying viewpoint is that a set of interactions is sufficient to understand both equilibrium and dynamic surface processes. Lattice-gas models provide a powerful and convenient route to explore how microscopic energies influence the statistical mechanics of nanoscale to sub-monolayer structures on crystalline surfaces. Such models underlie most Monte Carlo (and transfer matrix) simulations. They assume that overlayer atoms (or other adsorbed units) sit at particular high-symmetry sites of the substrate. The parameters

T.L. Einstein (✉)

Department of Condensed Matter Physics, University of Maryland, College Park,
MD 20742-4111, USA
e-mail: einstein@umd.edu

of the model are then the interaction energies between such atoms and/or the barriers associated with hops between the high-symmetry positions.

The use of lattice-gas models proceeds in two generic ways. In the first, one posits a few energies that are likely to dominate the physics of interest and then computes with Monte Carlo simulations the desired equilibrium or dynamic properties, deriving thereby the values of these energies from fits [1, 7, 8]. The dangers of this approach are (1) the properties of interest may be relatively insensitive to the specific interactions and (2) there may be other interactions that are non-negligible, so that the deduced energies are effective rather than actual.

The second approach [9–12] begins by actually computing the (many) energies of importance, a task that is now possible with efficient density functional theory packages such as VASP (the Vienna ab initio simulation package) [13, 14]. This process can be used to compute interaction energies between relatively distant neighbors. One should also compute multi-atom interactions, which can also be significant [3, 15]. As above, these interactions are then used in Monte Carlo simulations to test whether they account adequately for experimentally observed properties such as phase diagrams, equilibrium island shapes, or step fluctuations. This approach is appealing because the calculated interaction energies can be self-consistently checked for completeness, thereby mitigating the second danger mentioned above. Assuming that one has sufficient computational power to compute all the interactions that contribute at the level of the desired precision, there is still the danger that the interactions depend sensitively on the local environment, making a simple lattice-gas description inadequate. These caveats notwithstanding, lattice-gas models have been extensively used in the realm of surface physics to describe such diverse phenomena as phase transitions, phase diagrams, equilibrium island shapes, concentration-dependent diffusion, step fluctuations, and growth.

The basic assumptions that underlie lattice-gas models are as follows: (i) all atoms sit at high-symmetry positions and local relaxations produce the final structure; (ii) a finite set of effective interactions is sufficient to understand all the surface processes; and (iii) interactions are not sensitive to local positions of the adatoms. In the simplest scenario, only pair interactions between nearest neighbors are considered. However, in certain cases, like the orientation dependence of step stiffness and the equilibrium shape of islands, long-range pair interactions and multisite interactions are required for a complete description [8, 12, 16–20]. The substrates in these studies are typically mid- or late transition or noble metals, where the electronic indirect interaction leads to rich behavior [3].

Explicitly, the lattice-gas Hamiltonian of adatoms on a surface is written as

$$\mathcal{H} = \sum_{m=1}^M E_m \sum_{\langle ij \rangle_m} n_i n_j + \sum_T E_T \sum_{\langle ijk \rangle_T} n_i n_j n_k + \sum_Q E_Q \sum_{\langle ijkl \rangle_Q} n_i n_j n_k n_l + \dots \quad (2.1)$$

where n_i is the occupancy of the high-symmetry lattice site indexed i ; $n_i = 1$ denotes an occupied site; and $n_i = 0$ denotes an empty site. Interactions between adatom pairs up to the m th-neighbor pair E_m are included in the model (Fig. 2.1);

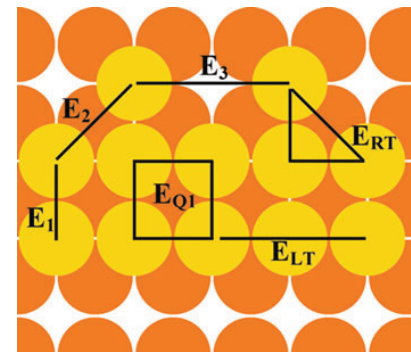


Fig. 2.1 Illustration of NN (nearest neighbor), NNN (next NN), and three NN (third NN) pairs with interaction energies E_1 , E_2 , and E_3 , respectively. Also shown are the isosceles right triangle (RT) with energy E_{RT} or, more formally, E_{112} (denoting a pair of NN legs and one NNN leg), and an isosceles linear triangle (LT) with energy E_{LT} or, more formally, E_{113} . Lastly, the most compact quato interaction has interaction energy E_{Q1} or, more formally, E_{1111} . For clarity [and physical relevance], here and in Fig. 2.5, the adatoms are placed in center sites, as for homoepitaxy on the (100) face of an fcc crystal like Cu, rather than atop sites as for homoepitaxy on a simple cubic crystal

accordingly, interactions between adatom pairs that are separated by distances greater than the m th neighbor distance are expected to be insignificant. E_T stands for three-adatom non-pairwise “trio” interactions, with the index running over all trimer configurations of significant strength. Similarly, E_Q stands for four-adatom non-pairwise (and with trios also subtracted) “quato” interaction. (The possibility of quato interactions has been known for over three decades [3, 21], but, to the best of our knowledge, it has been invoked only once in an actual calculation of adsorbate energetics [22]) until very recently [23, 24]. If necessary, pair interactions with a longer range and/or higher order multi-site interactions (possibly, five-adatom quintos) are included in the model till adequate convergence between theoretical predictions and experimental observations is obtained. However, the inclusion of a large number of interaction parameters makes the lattice-gas model intractable, thereby severely undermining the efficacy of lattice-gas models in characterizing overlayer systems.

The nature of the interactions leading to the lattice-gas pair energies has been reviewed extensively [3, 25–27] so we will present just a quick summary. If there is charge transfer (workfunction change) during the adsorption process, the adsorbates can interact electrostatically. Other “direct” interactions between the adatoms themselves can occur when the adatoms are at NN (nearest-neighbor) or perhaps NNN (next NN) sites. These are strong interactions, comparable to the binding energy, with the substrate playing a minor, sometimes negligible role; they are liable to produce relaxations that thwart straightforward application of lattice-gas models (cf. Sect. 2.5.2). When adatoms are sufficiently separated that there is insignificant overlap of the electron orbitals, there can still be an “indirect” interaction – weaker but

of longer range – mediated by substrate electrons or the elastic field. Elastic interactions tend to be of one sign and decay monotonically with adsorbate separation distance d , like d^{-3} asymptotically. They are generally taken to be isotropic, even when unjustified by the elastic tensor, since computing elastic Green's functions in the anisotropic case is notoriously difficult [28]. The electronic indirect interaction has richer behavior, oscillating in sign and reflecting the isotropy or anisotropy of the substrate wavefunctions in the surface plane [29]. Asymptotically it is dominated by the Fermi wavevector and has the Friedel behavior

$$d^{-n} \sin(2k_F d + \Phi) \quad (2.2)$$

where d is the [lateral] distance between the adsorbates; this result is non-perturbational, the phase factor Φ distinguishing it from the well-known perturbational RKKY expression [30]. (For a non-isotropic Fermi surface, the appropriate wavevector has *velocity* parallel to \mathbf{d} ; see [3] for details.) In the bulk, $n = 3$, but at a metal surface the leading term is canceled by that from its image charge, yielding $n = 5$. For trio interactions an expression similar to (2.2) holds to lowest order, with d replaced by the perimeter of the triangle formed by the adatoms. Here the decay is even faster, with $n = 7$. In short, interactions mediated by bulk states have negligible strength for values of d for which the asymptotic expression is valid.

The situation is strikingly different when there is a metallic surface state (i.e., a surface band that crosses the Fermi energy), such as found near the $\bar{\Gamma}$ point on the (111) faces of noble metals (associated with the (111) necks of the Fermi surface). For this case n is 2 and $5/2$ for pair and trio interactions, respectively, so that the asymptotic regime is physically important [31]. Indeed, trio interactions may play a role in the formation of 2D clusters of Cu/Cu(110) [32]. Furthermore, the Fermi “surface” is circular, and k_F is much smaller than its bulk counterpart, leading to the dramatic oscillations (with wavelength $\pi/k_F \approx 15 \text{ \AA}$) seen in STM experiments [33].

Most of the content of this and the second, third, and fifth sections of this chapter were included in the first author's presentation at the Vth Stranski-Kaischew Surface Science Workshop (SK-SSW'2005): “Nanophenomena at Surfaces – Fundamentals of Exotic Condensed Matter Properties” in Pamporovo, but have been updated. Each section provides references from which the content was adapted and from which more information can be obtained.

2.2 Recollection of Two Effects on Statistical Mechanics

In this section we recall two remarkable implications of trio interactions for phase diagrams [15]. While these ideas are not new, they have been largely ignored by the community and so bear repeating.

2.2.1 Pitfall in Transforming Trio Strength Between Lattice-Gas and Ising Models

Many researchers recast the lattice-gas model into an Ising model before doing computations. This seemingly innocent procedure invites pitfalls when multisite interactions are involved. Here we offer a particular example: what seems like a relatively modest three-spin interaction can correspond to an unphysically large trio interaction in the lattice-gas Hamiltonian. Our example involves a square lattice with $M = 2$ (first and second neighbor pair interactions) and the right-triangle trio E_{RT} corresponding to two E_1 legs at right angles and an E_2 hypotenuse (or E_{112} for short, in a general formal notation [3]).

The mapping to spin language, with $s_i = \pm 1$, is $n_i = (1 + s_i)/2$. We see

$$\mathcal{H} = \left(\frac{E_1}{4} + \frac{E_{RT}}{2} \right) \sum_{(ij)_1} s_i s_j + \left(\frac{E_2}{4} + \frac{E_{RT}}{4} \right) \sum_{(ij)_2} s_i s_j + \frac{E_{RT}}{8} \sum_{(ijk)_{RT}} s_i s_j s_k \quad (2.3)$$

In Ising or spin language, the three coefficients are called $-J_1$, $-J_2$, and $-J_{RT}$, respectively. For the pair interactions, we easily see that

$$\frac{J_2}{J_1} = \frac{E_2/E_1 + E_{RT}/E_1}{1 + 2E_{RT}/E_1} \approx \frac{E_2}{E_1} \text{ for } |E_{RT}| \lesssim 4|E_1| \quad (2.4)$$

One might then naively – but incorrectly – expect that $J_{RT}/J_1 \approx E_{RT}/E_1$. Instead

$$\frac{J_{RT}}{J_1} = \frac{E_{RT}/E_1}{2 + 4E_{RT}/E_1} \Leftrightarrow \frac{E_{RT}}{E_1} = \frac{2J_{RT}/J_1}{1 - 4J_{RT}/J_1} \quad (2.5)$$

This highly non-linear relation leads to a surprising result: For $J_{RT}/J_1 \lesssim 1/4$, $E_{RT}/E_1 \gg J_{RT}/J_1$. Furthermore, if J_{RT}/J_1 increases to slightly above $1/4$, E_{RT}/E_1 becomes large and negative. A similar effect would occur in the opposite direction for $E_{RT}/E_1 \approx -1/2$, a larger magnitude than one is likely to encounter.

Finally, it is unfortunate (to say the least) that some researchers (including prominent ones) denote the lattice-gas energy parameters as J . Even in the simplest case of just a nearest-neighbor interaction, the lattice-gas energy differs from the Ising energy by a factor of 4; thus, misinterpretation and numerical inaccuracies are very likely.

2.2.2 Effect on Phase Boundaries: Asymmetries Not Inevitable

A trio interaction, which breaks particle–hole symmetry (or up–down symmetry in the Ising viewpoint), is generally expected to lead inevitably to substantial asymmetries in phase diagrams about half-monolayer coverage. A rather surprising finding of numerical [Monte Carlo] calculations is that a single type of trio interaction need

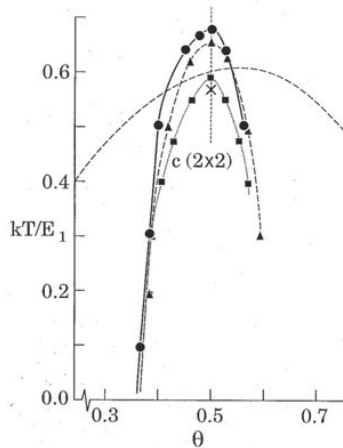


Fig. 2.2 Illustration, for a $c(2 \times 2)$ overlayer on a square lattice, of the heuristic guideline, based on scaling the elementary excitation, used to predict which trios produce observable asymmetries in phase boundaries. For the simplest case of an NN repulsion, E_1 , the disordering temperature is known exactly from the Onsager solution to the Ising model; it is indicated by the \times on the temperature-coverage phase diagram. The effect of adding a right-triangle trio repulsion E_{RT} , a linear trio repulsion E_{LT} , or both was studied using Monte Carlo for the case $E_{RT} = E_{LT} = E_1/4$; the results for the three cases are plotted with *filled triangles, squares, and circles*, with *dashed, dotted, and solid curves*, respectively, added to guide the eye. The behavior at $\theta = 0.5$ is anticipated by (2.7) and (2.8). The *dashed and dotted curves* appear symmetric about $\theta = 0.5$ (*short-dotted line*); only with both trios present does the [*solid*] phase boundary become noticeably asymmetric. In the plots at the right, the \times 's and dots indicate occupied and vacant sites, respectively, in a perfectly ordered configuration, with the large symbols denoting a vacancy ($\theta < 1/2$) or extra adatom ($\theta > 1/2$), respectively. The *arrows* on the plots depict the lowest energy excitations, with the linetype of the shaft corresponding to the linetype of the phase boundary on the phase diagram; for each linetype, this excitation energy is the same for $\theta < 1/2$ and $\theta > 1/2$. According to the heuristic prescription, these energies scale the disordering temperature. When both trios are present, there is “frustration” over which excitation to use, the prescription fails, and asymmetries occur. In the phase diagram, the *broad dashed curve* is the result of a mean-field calculation, plotted at half its magnitude (i.e., $T_c(\theta = 0.5) \approx 1.2E_1$); not only is this prediction of T_c far too high and too broad, it also erroneously predicts substantial asymmetry. From [15]

not necessarily do so. (See also the discussion by Persson of the role of adsorption in sites not of high symmetry, the equivalence to trio interactions, and the rich effects on temperature-coverage phase diagrams [2, 34].) This result, illustrated in Fig. 2.2 for the case of a $c(2 \times 2)$ overlayer with $E_1 > 0$ and E_{RT} , is in sharp contrast to the observation in 2D calculations which treat fluctuations approximately – mean-field and quasi-chemical approximations – that trios must produce such asymmetries [35]. Likewise we see that a linear trio E_{LT} alone does not produce an asymmetry. However, when both E_{RT} and E_{LT} are present, the expected notable asymmetry does appear. To comprehend this effect of trios on the phase boundary, we need some way to assess the difference in the way the trio interactions affect the lower temperature

ordered phase compared to the higher temperature disordered phase. Evidently the breaking by trios of the particle–hole symmetry of the pair interaction lattice-gas hamiltonian, and the resulting asymmetry in the ground state energy, is not the crux.

We describe a crude approximation scheme for assessing the change in the disordering temperature T_c of an ordered phase from a known value $T_c(0)$ for some Hamiltonian to $T_c(E_{\text{new}})$ for a more complicated Hamiltonian with a new interaction energy E_{new} . While we have applied our procedure [36] to a wide range of problems, we still have no formal derivation. In essence, the idea is that T_c scales with the lowest energy excitation from the ground state. In [36] we show, e.g., that for a $c(2 \times 2)$ overlayer with half-monolayer coverage, characterized by a nearest-neighbor repulsion E_1 and a smaller second-neighbor interaction E_2 ,

$$T_c(E_2) = T_c(E_2 = 0) \left(1 - \frac{4E_2}{3E_1} \right) \quad (2.6)$$

For this simple problem, Barber [37] showed that the exact coefficient is $\sqrt{2} \approx 1.41$ rather than $4/3 \approx 1.33$; on the other hand, our value is much better than the mean-field prediction of 1. For this same problem, the effect of a right-triangle trio interaction E_{RT} (with $E_2 = 0$) is given by

$$\frac{3E_1 + 2E_{RT}}{T_c(E_{RT})} = \frac{3E_1}{T_c(0)} \Rightarrow T_c(E_{RT}) = T_c(E_{RT} = 0) \left(1 + \frac{2E_{RT}}{3E_1} \right) \quad (2.7)$$

Similarly, for a linear trio E_{LT}

$$\frac{3E_1 + E_{LT}}{T_c(E_{LT})} = \frac{3E_1}{T_c(0)} \Rightarrow T_c(E_{LT}) = T_c(E_{LT} = 0) \left(1 + \frac{E_{LT}}{3E_1} \right) \quad (2.8)$$

We caution that this procedure is applicable only if the new interaction does not alter the symmetry of the ordered state and works well only if the nearby elementary excitation from the fully ordered state is uniquely defined. Thus, it works well for a $(\sqrt{3} \times \sqrt{3})$ overlayer on a hexagonal net but not for a $p(2 \times 2)$. It is also curious that this procedure requires a lattice-gas picture in which the number of atoms is conserved (i.e., a canonical ensemble or Kawasaki dynamics); if the atom instead hopped to a “bath” (i.e., a grand canonical ensemble, or fixed chemical potential, or a single spin flip in a spin analogue (Glauber dynamics)), the predictions are quite poor.

To assess the effect of trios on the symmetry of the temperature-coverage phase boundary of a $c(2 \times 2)$ overlayer, we look at the elementary excitation near a defect, either an extra adatom or a missing one (see Fig. 2.2). For just a right-triangle trio, there are no such trios (no $2E_{RT}$) in the excited state when there is a vacancy; when there is an extra adatom, there are two RT trios in the ordered state which are lost in hopping to the nearest neighbor (where another two RT trios occur). So in both cases, there is no change in the number of RT trios, i.e., no change proportional to E_{RT} is involved. A similar effect occurs with a linear trio, but with a different

elementary excitation (see Fig. 2.2). In either case, we saw that the phase boundary computed using Monte Carlo appears symmetric. Only when both trios are present does a marked asymmetry occur. However, a noteworthy inadequacy of this simple picture is its inability to give any idea of the coverage dependence of T_c (M.E. Fisher, private communication).

2.3 Applications to Gases on Metals

As an example of the state of the art in quantitatively determining adsorbate–adsorbate interactions from combined theory and experiment, we discuss the study of $c(2 \times 2)N$ on Fe(001) by Österlund et al. [8]. Since there is just one ordered phase, one might expect to be able to extract information about only a handful of interactions, say $E_1 > 0$, E_2 , and a trio, from STM observations. The authors use a new concept called configuration distribution analysis (CDA) to extract much more information from high-resolution images. Around each nitrogen adatom they obtain a site map of possible adsorption sites. By comparing the resulting experimental conditional probabilities with those obtained from Monte Carlo simulations with a lattice-gas model, they can refine estimates of the various interactions.

The authors first consider a long-established analysis [38, 39] of the pair correlation function $g(j)$, from which they deduce $E_j = -k_B T \ln g(j)$, for j th neighbors, between fractional coverages $\Theta = 0.037$ and 0.15. They find very little NN site occupation and enhanced NNN occupation. For $j > 4$ there is no significant deviation from a random distribution ($g = 1$). From the data they find $E_1 = 0.13$ eV and $E_2 = -0.013$ eV. Concerned about poor statistics at $\Theta = 0.037$, the authors also carried out Monte Carlo simulations and used a least-squares fit of data at all the coverages, finding similar energies: $E_1 = 0.14$ eV, $E_2 = -0.023$ eV, and $E_3 = 0.003$ eV. They then did a CDA analysis in conjunction with Monte Carlo simulations (seemingly at $\Theta = 0.108$), supplemented by a comparison of measured and simulated island-size distributions. They thus determined $E_1 = 0.13$ eV, $E_2 = -0.018$ eV, $E_3 = 0.019$ eV, and trio interaction energies $E_{223} = -0.012$ eV, and $E_{225} = 0.006$ eV. (These trios correspond to RT and LT triangles on a larger scale, with insignificant direct interactions.) If 3NN (third NN) sites are considered in the CDA, then E_3 decreases to 0.015 eV. If trios are omitted from the CDA analysis, E_1 is unchanged but E_2 increases in magnitude to -0.038 eV, while E_3 diminishes to 0.003 eV. In other words, fitted pair interactions are actually effective interactions that include omitted interactions in some average, unspecified way. The effect seems to be largest for the most prominent legs of the omitted interactions, in this case NNN.

The authors also include an elastic repulsion, taken to have the asymptotic isotropic form C/R^3 with strength $C/a^3 = 0.15$ eV, where a is the Fe lattice constant (2.87 Å). Hence, the *electronic* components of the three pair interactions (for the CDA analysis including trios and configurations to $j = 3$) are -0.2 , -0.71 , and -0.04 eV, respectively. (There is no comment about adjusting the trios.) Note, remarkably, that $|E_1^{\text{el}}| < |E_2^{\text{el}}|$. The authors conclude that the electronic interaction

is short range. The embedded atom method (EAM), for metals on metals, predicts that the indirect interaction is repulsive and proportional to the number of shared substrate atoms [3]. On very general grounds one expects R^{-5} decay of the envelope in (2.2). We caution that the distinction between electronic and elastic has long been recognized as subtle [40] and that the asymptotic limit of the elastic interaction is likely to be significantly modified at separations $\mathcal{O}(a)$ by more rapidly decaying terms in the multipole series [41].

2.4 Refined Schemes for Extracting Interaction Energies

To extract estimates of interaction energies when there are many such parameters are a delicate task typically one obtains a large number of simultaneous equations by computing the total interaction of a large variety of different overlayer structures. One should have more overlayer structures than interactions so as to be able to check for robustness of the deduced values. While informal schemes had formerly seemed sufficient [42], it is safer and sounder to use formal cross-validation schemes used by several groups [12, 43] to study overlayer systems.

In recent work [44] we used the leave- n_v -out cross-validation method [45] to fit the computed energies for Cu(110) to the interaction parameters (cf. Sect. 2.6). This method is expected to perform better than the more commonly used leave-one-out cross-validation scheme [45]. We calculated the interaction strengths in the following way: for a particular supercell, we computed total energies for, say, n different configurations of adatoms. In addition, we posit the number of significant interactions n_i . We then use n_i (out of n) equations to solve for the interaction energies. These interactions are then used to predict the energies of the remaining $n_v = n - n_i$ equations. We then compute the root mean squared (rms) of the prediction error per adatom for all configurations j ($1 \leq j \leq n_v$), each with a_j adatoms in it:

$$\Delta E_{\text{rms}} = \sqrt{\frac{1}{n_v} \sum_{j=1}^{n_v} (\Delta E_j)^2} \quad \Delta E_j = \frac{E^{\text{pred}} - E^{\text{VASP}}}{a_j} \quad (2.9)$$

We repeat this procedure for different partitions of (n, n_i) , and sets of interactions from only those partitions whose ΔE_{rms} values are lower than a specified threshold value (10 meV/adatom in Ref. [44]) are considered for the final averaging of interaction values. Finally, we find the value of n_i that leads to the best convergence. As a check, we perform this procedure on two different computational supercells.

2.5 Effect of Relaxations in Homoepitaxy with Direct Lateral Interactions

When direct interactions play a significant role, such as for (1×1) homoepitaxial partial monolayers, one must be wary of relaxation-induced modification of

energies near steps or island edges. From bond energy, bond order, bond length reasoning [46], one can expect such atoms – which lack their full complement of near-neighbor bonds, to move closer to the remaining neighbors to partially compensate for the loss. Persson showed that relaxation in the form of adsorption away from high-symmetry sites can lead to effective trio interactions, and attendant effects, in systems with ostensibly only pair interactions [2, 34]. Our goal here is to show that these relaxation effects are especially significant for multisite interactions, where the relaxations are not along the bond directions. Furthermore, multisite interactions, in general, have a large elastic component; hence, a careful consideration of relaxation effects is needed while computing them. We discuss in particular how strain-related effects are important when calculating the step stiffness on Cu(100). Because of adatom relaxation near steps, the inclusion of non-pairwise, quarto interaction between four adatoms is required on this square-lattice surface in order to preserve a lattice-gas description.

2.5.1 Multisite Interactions in Step-Stiffness Asymmetry

Step stiffness (which earlier served as the mass in the 1D fermion model of steps) underlies how steps respond. It is one of the three parameters of the step-continuum model [47], which has proved a powerful way to describe step behavior on a coarse-grained level, without recourse to a myriad of microscopic energies and rates. In the analogy between 2D configurations of steps and worldlines of spinless fermions in $(1+1)\text{D}$, step stiffness $\tilde{\beta}$ plays the role of the mass of the fermion. As the inertial term, stiffness determines how a step responds to fluctuations, to driving forces, and to interactions with other steps.

We summarize our lattice-gas-based computations of the orientation dependence of step stiffness for the (001) and (111) faces of Cu [48, 49]. This work illustrates both successes and some shortcomings of using a lattice-gas model with just NN interactions: whereas the step stiffness on Cu(111) is well described by NN interactions alone, the step stiffness on Cu(001) requires the inclusion of NNN and perhaps even trio interactions. We discuss only the latter.

The step stiffness $\tilde{\beta}(\theta) \equiv \beta(\theta) + \beta''(\theta)$ weights deviations from straightness in the step Hamiltonian, where θ is conventional designation of the azimuthal misorientation angle; it measured from the close-packed direction. Here β is the step-free energy per length (or, equivalently, the line tension, since the surface is maintained at constant [zero] charge [50]). The stiffness is inversely proportional to the step diffusivity, which measures the degree of wandering of a step perpendicular to its mean direction. This diffusivity can be readily written down in terms of the energies ε_k of kinks along steps with a mean orientation $\theta = 0$: in this case, all kinks are thermally excited. Conversely, experimental measurements of the low-temperature diffusivity (via the scale factor of the spatial correlation function) can be used to deduce the kink energy. A more subtle question is how this stiffness depends on θ . Even for temperatures much below ε_k , there are always a non-vanishing number

of kinks when $\theta \neq 0$, the density of which is fixed by geometry (and so are proportional to $\tan \theta$). In a bond-counting model, the energetic portion of the $\beta(\theta)$ is canceled by its second derivative with respect to θ , so that the stiffness is due to the entropy contribution alone. Away from close-packed directions, this entropy can be determined by simple combinatoric factors at low temperature T [51–53].

Interest in this whole issue has been piqued by Dieluweit et al.’s finding [54] that the stiffness as predicted in the above fashion, assuming that only NN interactions E_1 are important, underestimates the values for Cu(001) derived from two independent types of experiments: direct measurement of the diffusivity on vicinal Cu surfaces with various tilts and examination of the shape of (single-layer) islands. The agreement of the two types of measurements assures that the underestimate is not an anomaly due to step–step interactions. In that work, the effect of NNN interactions E_2 was crudely estimated by examining a general formula obtained by Akutsu and Akutsu [55], showing a correction of order $\exp(-E_2/k_B T)$, which was glibly deemed to be insignificant. In subsequent work the Twente group [56] considered steps in just the two principal directions and showed that by including an attractive NNN interaction, one could evaluate the step-free energies and obtain a ratio consistent with the experimental results in [54]. They later extended their calculations [57] to examine the stiffness.

To make contact with experiment, one typically first gauges the diffusivity along a close-packed direction and from it extracts the ratio of the elementary kink energy ε_k to T . Arguably the least ambiguous way to relate ε_k to bonds in a lattice-gas model is to extract an atom from the edge and place it alongside the step well away from the new unit indentation, thereby creating four kinks [58]. Removing the step atom costs energy $3E_1 + 2E_2$ while its replacement next to the step recovers $E_1 + 2E_2$. Thus, whether or not there are NNN interactions, we identify $\varepsilon_k = -\frac{1}{2}E_1 = \frac{1}{2}|E_1|$ (since the formation of Cu islands implies $E_1 < 0$); thus, as necessary, $\varepsilon_k > 0$.

In the low-temperature limit, appropriate to the experiments [54], we have shown that

$$\frac{k_B T}{\tilde{\beta} a} = \frac{m \sqrt{(1-m)^2 + 4me^{E_2/k_B T}}}{(1+m^2)^{3/2}} \xrightarrow{m \rightarrow 0^+} \frac{m+m^2}{(1+m^2)^{3/2}} \quad (2.10)$$

where m is the step-edge in-plane slope.

Figure 2.3 compares (2.10) to corresponding exact solutions at several temperatures when $E_2 = E_1/10$. We see that (2.10) overlaps the exact solution at temperatures as high as $T_c/6$. As the temperature increases, the stiffness becomes more isotropic, and (2.10) begins to overestimate the stiffness near $\theta = 0^\circ$. In Fig. 2.4 (using the experimental value [59] $\varepsilon_k = 128 \text{ meV} \Rightarrow E_1 = -256 \text{ meV}$), we compare (2.10) to the NN Ising model at $T = 320 \text{ K}$, as well as to the experimental results of [54]. For strongly attractive (negative) E_2 , $k_B T/\tilde{\beta} a$ decreases significantly. In fact, when E_2/E_1 is 1/6, so that $-E_2/2k_B T = (E_2/E_1)(\varepsilon_k/k_B T) \approx (1/6)4.64$, the model-predicted value of $k_B T/\tilde{\beta} a$ has decreased to less than half its $E_2 = 0$ value, so about 3/2 the experimental ratio. For the NNN interaction alone to

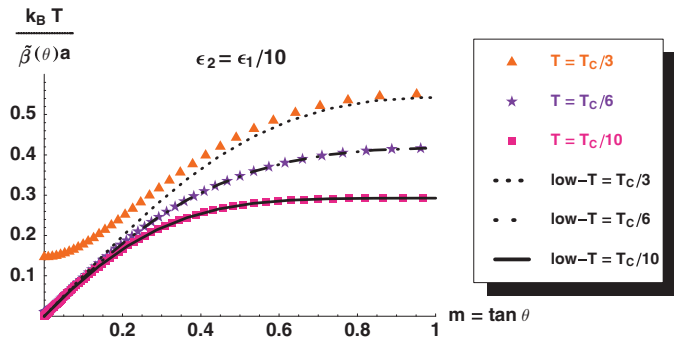


Fig. 2.3 The range of validity of (2.10) is examined by comparing it to exact numerical solutions of the SOS model at several temperatures. In the legend T_c refers to the NN lattice-gas (Ising) model; for $|E_1| = 256$ meV, $T_c = 1685$ K. From [48]

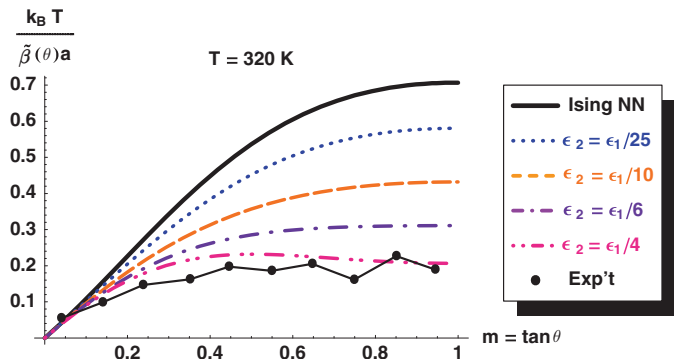


Fig. 2.4 Equation (2.10) is plotted for a range of values of E_2 (ϵ_2 on the plot, where E_1 and E_2 are NN and NNN interaction energies, respectively, in a lattice-gas picture). The *solid curve* denoted “Ising NN” corresponds to $E_2 = 0$. The *dots* labeled “Exp’t” are taken from figure 2 of [54] and were derived from the equilibrium shape of islands on Cu(001) at 302 K, with line segments to guide the eye. To clarity, we omit similar data derived from correlation functions of vicinal surfaces at various temperatures. Note that for $E_2 = E_1/4$ there is a maximum near $\tan \theta = 1/2$ that is not observed in experimental data. From [48]

account for the factor-of-4 discrepancy between model/theory and experiment [54], Fig. 2.4 shows that $E_2/E_1 \approx 0.3$ would be required.

2.5.2 Effect of Trio Interactions

If we include an RT trio (E_{112}) the effective NN lattice-gas energy E_1^{eff} is $E_1 + 2E_{\text{RT}}$ and more significantly the effective NNN interaction energy is $E_2 + E_{\text{RT}}$. Thus, E_{RT} must be attractive (negative) if it is to help account for the discrepancy in

figure 2 of [54] between the model and experiment. Furthermore, by revisiting the configurations discussed in the penultimate paragraph of the Introduction, we find that the kink energy ϵ_k becomes $-\frac{1}{2}E_1 - E_{\text{RT}}$. Thus, for a repulsive E_{RT} , $|E_1|$ will be larger than predicted by an analysis of, e.g., step-edge diffusivity that neglects E_{RT} . Lastly, the close-packed edge energy, i.e., the $T = 0$ line tension $\beta(0) = -\frac{1}{2}E_1 - E_2$, becomes $-\frac{1}{2}E_1 - E_2 - 2E_{\text{RT}}$.

We also investigated the strain-related effects on calculated trio interaction energies on Cu(100), where Dieluweit et al. [54] showed that the NN Ising model cannot explain the experimentally observed step-stiffness anisotropy. In a response, we showed that the addition of an effective NNN attractive interaction could resolve the discrepancy. The effective NNN interaction (E_2) can be written as the sum of two components as illustrated in Fig. 2.5a:

- a pairwise second neighbor interaction energy (E_2)
- an orientation-dependent right-isosceles trio interaction energy (E_{RT})

However, when we used VASP to calculate these interactions, we found a large repulsive value of around 50 meV for the right-isosceles trio interaction energy (E_{RT}). Such a value cancels the calculated attractive second-neighbor interactions (E_2) thereby reducing the model to an NN Ising model. Thus, in the end the discrepancy between theory and experiment could not be resolved.

To see the effect of relaxation, we repeated the calculations with a bigger supercell ($4 \times 4 \times 14$). If an adatom stripe has kinks, there can be two types of right-isosceles trios, ones with one/two adatoms on the step-edge and ones with no adatoms on the step edge (Fig. 2.5b). Since the local geometry of these two adatoms is different, we could expect the trio interaction energies to be different because the RT trio adatoms (E_{RT}') inside a stripe cannot relax as much laterally as the trios with its vertices on the step (E_{RT}). The trio energy that we calculated earlier corresponds to a linear combination of E_{RT} and E_{RT}' , weighted more dominantly by E_{RT}' . However, the calculation of the step stiffness depends on broken step-edge trios, which necessarily correspond to E_{RT} . To distinguish these two trios here, we calculated the

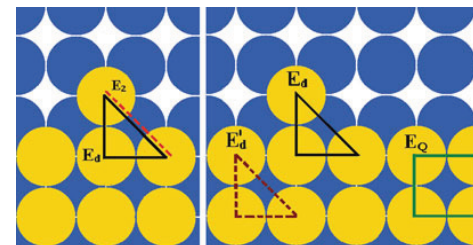


Fig. 2.5 (a) Effective NNN interactions on a (100) surface [of an fcc crystal], (b) multisite interactions E_d (*solid triangle*), E_d' (*broken triangle*), and E_Q (*square*), where the subscript d is RT in our notation. The trio E_d has adatoms on the step edge whereas E_d' has no adatoms on the step edge. From [23]

energies of four different adatom configurations and we solved the resultant linear system of equations. With this correction, at the step-edge $E_{RT} \approx 12.5$ meV/atom, and the effective NNN interaction is thus $E_2^{\text{eff}} = E_2 + E_{RT} \approx -35$ meV/atom.

Though E_{RT} is still repulsive, its magnitude is lower than that of the attractive E_2 . The ratio of the effective NN interaction to the effective NNN interaction is

$$E_2^{\text{eff}}/E_1^{\text{eff}} \sim 1/9 \quad \text{while} \quad E_2/E_1 \sim 1/7 \quad (2.11)$$

which is much closer to experimental expectations.

Distinguishing between the step-edge trios E_{RT} and the bulk trios E'_{RT} is not compatible with a proper lattice-gas picture, where interactions should not depend on local position and geometry. We can remedy this problem by introducing a quarto interaction. This quarto interaction distinguishes between the two trios because it is present only in bulk trios E'_{RT} :

$$E'_{RT} = (3/4)E_Q + E_{RT} \quad (2.12)$$

This yields the value of the quarto interaction to be $E_Q = 53$ meV. This is a significant amount of energy (compared with collinear trio $E_{LT} = -15$ meV/atom and third-nearest-neighbor interaction $E_3 = -8$ meV/atom [60]) and hence is likely to have consequences in calculations of other properties.

In summary, when calculating trio interactions from first principles, however, care must be taken; they can be exquisitely sensitive to the geometry and structure of the supercell used to calculate them. Such sensitivity to local relaxation can complicate a simple lattice-gas description. To account for the relaxation of trios near step edges, for example, we introduce a non-pairwise quarto interaction E_Q among four neighboring adatoms. We find that such an interaction is necessary to bridge the theoretical step stiffness with experimental measurements on Cu(100). In that case, we find what amounts to a relatively large, repulsive quarto interaction $E_Q = 53$ meV that has significant physical consequences in our problem and presumably more generally. (In the same paper [23] we find that the inclusion of trio interactions can account for the difference in A- and B-step formation energies on Pt(111).)

2.6 Connector Models

The expansion in m -adatom interactions can become cumbersome and unwieldy if the multiparticle energies do not become smaller after, say, quarto interactions. Seeking an alternative approach to circumvent this issue, Tiwary and Fichthorn (TF) [24] proposed the connector model (named after the construction-kit toy [61]), which focuses on the vertices rather than the links of a cluster of adatoms. For example, consider four adatoms forming an NN square. In the lattice-gas model, the total energy would be $4E_1 + 2E_2 + 4E_{RT} + E_Q$. In the connector model with just NN spokes (spokes of half the NN bond length and oriented in the appropriate

directions), this total energy is just four times the energy of a connector hub with two perpendicular spokes. For this lattice, there are just five types of connectors, having one, two, three, or four spokes, the two-spoke case having a straight and a right-angle conformation. More often, one must use connectors with NN and NNN spokes. For the square of four adatoms, there would still be just one connector, with an NNN spoke between the two perpendicular NN spokes (called D6 in [24]). For the straight-conformation two NN spoke case, one can add one NNN spoke in one distinct conformation, two NNN spokes in three conformations, three or four (or 0) each in one distinct conformation, summing to seven possibilities. In other cases there will be even more. With three NN spokes, the number of possibilities is even larger. One of the main features of this model is that the type of connector contains information about the local geometry of the adatom; hence relaxation effects are expected to be built into the model. However, to keep the number of fitted energies reasonable, TF use just eight connectors: D1 for an isolated atom; D2 and D3 for just one NN or NNN spoke, respectively; D4 and D5 for two NN or NNN spokes in the same direction (linear), respectively; D7 with three NN spokes and two NNN spokes between them; and D8 for all eight spokes. Thus, as for lattice-gas interactions, success requires that the investigator have enough insight into the system to select the connectors that capture the essence of the problem.

Other applications to date have been to (110) fcc surfaces, where the rectangular symmetry leads to a large variety of lattice-gas energies as well as a much greater number of connectors, since the perpendicular ‘‘NN’’ spokes have different lengths (though NNN are still the same). However, the multiplicity can be reduced by sometimes neglecting some differences. We used 10 connectors (shown in Fig. 2.6) to characterize adatom interactions on Cu(110) [44], while TF used the first nine for Al(110).

For Cu(110) the CV scores are as good as those obtained using a dozen lateral interactions in the lattice-gas approach [44]. This agreement is plausible since it is often possible to establish linear relations between the connector and lattice-gas energies, e.g.,

$$C_6 = E_0 + \frac{E_1}{2} + \frac{E_2}{2} + \frac{E_3}{2} + \frac{E_{T1}}{3} + \frac{E_{Q1}}{4} \quad (2.13)$$

The sensitivity of multisite interactions to relaxation is not apparent from the connector energy values because each connector has contributions from adsorption energy (E_0 or C_1) and other pairwise interactions that dominate over contributions from multisite interactions; also, the contribution from a particular multisite interaction is divided by the number of participating adatoms (cf. (2.13), further decreasing the sensitivity of connector energies to adatom relaxations. However, the connector model incorporates such relaxation effects, as can be seen from the uniformly low CV scores for all relaxation schemes [44]. Evidently the connector model works well in the cases of Cu(110), Al(110), and Al(100). It remains to be seen whether the connector model provides an adequate solution, without the need for any ad hoc patches, to the overlay problem. Relaxation effects become prominent during

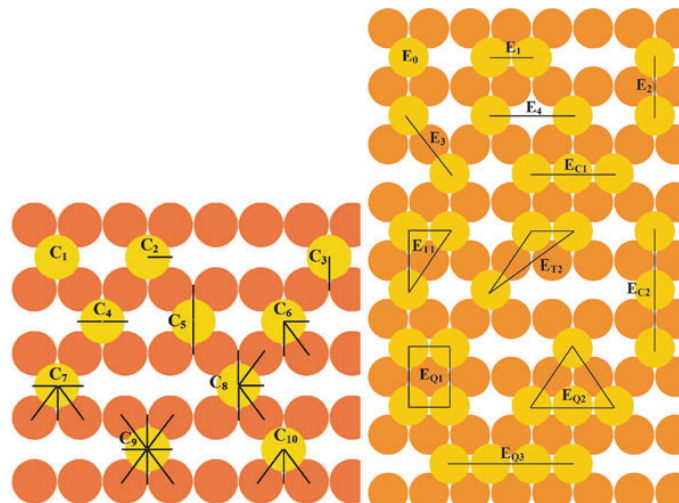


Fig. 2.6 *Left:* Connectors [24] used to characterize Cu adatom interactions on Cu(110). *Lighter (mustard) circles* represent adatoms and *darker (orange) circles* represent atoms in the substrate layer. *Right:* Lattice-gas interactions used to characterize Cu adatom interactions on Cu(110). Multisite interactions E_{T2} , E_{Q2} , and E_{Q3} were found to be insignificant. From [44], which also provides tables of the values of these energies

energy calculations of adatoms near step edges; in such calculations the simple lattice-gas model encounters problems [23, 60]. At the same time, accommodating the relaxation effects encountered in such calculations within the connector model might require the usage of connectors that account for the orientations of neighbor bonds, resulting in an undesirably large number of connectors in the model. A DFT-based study that compares these two models on a surface like Pt(111), where such lateral relaxation is known to complicate surface energy calculations [23], might elucidate this issue.

2.7 Interactions Between Organic Molecules

Understanding the interactions between and consequent self-assembly of organic molecules on metal surfaces has drawn much recent interest. The adsorption bond is roughly an order of magnitude weaker than for the chemisorbed systems considered above. Direct interactions between the organic molecules are often by way of hydrogen bonds, and there is always a van der Waals attraction which, for these systems, may play the dominant role. While the coupling to the substrate is relatively weak, the indirect electronic interactions between adsorbates may be important at long range when the substrate has metallic surface states.

Very recently we have considered the adsorption of benzene on Cu(111) [62], using a DFT approach with a van der Waals functional included. We can account for the two ordered submonolayer phases observed by Dougherty et al. [63]. The denser phase is due to direct van der Waals bonding between the benzenes while the less dense phase appears to be due to the surface-state-mediated interaction. We have not yet investigated the role of trio interactions in this system. Our ultimate goal is to explain the dramatic giant regular honeycomb structure formed by anthraquinone (AQ) molecules on this substrate [64]. In models that treat the adatoms as single “atoms,” a repulsive trio interaction is crucial to prevent the formation of dense, unphysical overlayer regions (Kim and Einstein, Unpublished). Our belief is that the large, regular structure is related to interactions between AQ mediated by the metallic surface state. A variety of theoretical and experimental techniques are in progress to confirm this picture (Bartels and Einstein, Unpublished).

Acknowledgments Our research at Maryland was supported primarily by the NSF-MRSEC, Grant DMR 05-20471. Some aspects benefited from NSF Grant Chem 07-50334 and DOE-CMSN support. The Center for Nanophysics and Advanced Materials (CNAM) provided ancillary support. We thank T.J. Stasevich, P. Hyldgaard, K. Berland, E.D. Williams, L. Bartels, and K. Kim for fruitful collaboration and stimulating discussions on the topics discussed.

References

1. L.D. Roelofs, in *Chemistry and Physics of Solid Surfaces, IV*, ed. by R. Vanselow, R. Howe (Springer, Berlin, 1982), p. 219
2. B.N.J. Persson, *Surface Sci. Rept.* **15**, 1 (1992)
3. T.L. Einstein, in *Physical Structure of Solid Surfaces*, ed. by W.N. Unertl (Elsevier, Amsterdam, 1996), p. 577
4. A. Patrykiewicz, S. Sokolowski, K. Binder, *Surf. Sci. Rept.* **37**, 207 (2000)
5. D.P. Landau, S.P. Lewis, H.-B. Schüttler (ed.), *Computer Simulation Studies in Condensed-Matter Physics*, vols. 1–19 (Springer Proceedings in Physics, Berlin, 1988–2008)
6. P.A. Rikvold, G. Brown, M.A. Novotny, A. Wieckowski, *Colloids Surf. A: Physicochem. Eng. Asp.* **134**, 3 (1998)
7. L.D. Roelofs, in *Physical Structure of Solid Surfaces*, ed. by W.N. Unertl (Elsevier, Amsterdam, 1996), p. 713
8. L. Österlund, M.Ø. Pedersen, I. Stensgaard, E. Lægsgaard, F. Besenbacher, *Phys. Rev. Lett.* **83**, 4812 (1999)
9. A. Bogicevic, S. Ovesson, P. Hyldgaard, B.I. Lundqvist, H. Brune, D.R. Jennison, *Phys. Rev. Lett.* **85**, 1910 (2000)
10. J.-S. McEwen, S.H. Payne, C. Stampfl, *Chem. Phys. Lett.* **361**, 317 (2002)
11. W. Luo, K.A. Fichthorn, *Phys. Rev. B* **72**, 115433 (2005)
12. C. Stampfl, *Catal. Today* **105**, 17 (2005); M. Borg et al., *Chem. Phys. Chem.* **6**, 1923 (2005)
13. G. Kresse, J. Hafner, *Phys. Rev. B* **47**, R558 (1993); **49**, 14251 (1994)
14. G. Kresse, J. Furthmüller, *Comput. Mater. Sci.* **6**, 15 (1996); *Phys. Rev. B* **54**, 11169 (1996)
15. T.L. Einstein, *Langmuir* **7**, 2520 (1991)
16. G. Ehrlich, F. Watanabe, *Langmuir* **7**, 2555 (1991)
17. S.-J. Koh, G. Ehrlich, *Phys. Rev. B* **60**, 5981 (1999)
18. Y. Zhang, V. Blum, K. Reuter, *Phys. Rev. B* **75**, 235406 (2007)
19. Y. Tiwary, K.A. Fichthorn, *Phys. Rev. B* **75**, 235451 (2007)

20. C. Lazo, F.J. Keil, Phys. Rev. B **79**, 245418 (2009)
21. W.A. Harrison, Phys. Rev. B **7**, 2408 (1973)
22. L.D. Roelofs, S.M. Foiles, M.S. Daw, M.I. Baskes, Surf. Sci. **234**, 63 (1990)
23. R. Sathiyarayanan, T.J. Stasevich, T.L. Einstein, Surface Sci. **602**, 1243 (2008)
24. Y. Tiwary, K.A. Fichtorn, Phys. Rev. B. **78**, 205418 (2008)
25. T.L. Einstein, in *Chemistry and Physics of Solid Surfaces II*, ed. by R. Vanselow (CRC Press, Boca Raton, FL, 1979), p. 181
26. P.J. Feibelman, Ann. Rev. Phys. Chem. **40**, 261 (1989)
27. J.K. Nørskov, in *The Chemistry and Physics of Solid Surfaces*, vol. 6, ed. by D.A. King, D.P. Woodruff (Elsevier, Amsterdam, 1993), p. 1
28. S.P. Timoshenko, J.N. Goodier, *Theory of Elasticity*, 3rd edn. (McGraw-Hill, New York, NY, 1970)
29. T.L. Einstein, J.R. Schrieffer, Phys. Rev. B **7**, 3629 (1973)
30. C. Kittel, in *Solid State Physics*, ed. by F. Seitz, D. Turnbull, H. Ehrenreich (Academic, New York, NY, 1968), vol. 22, p. 1, and references therein.
31. P. Hyldgaard, M. Persson, J. Phys. Condens. Matter **12**, L13 (2000); P. Hyldgaard, T.L. Einstein, Europhys. Lett. **59**, 265 (2002)
32. P. Hyldgaard, T.L. Einstein, Surf. Sci. **532–535**, 600 (2003); J. Cryst. Growth **275**, e1637 (2005)
33. M.F. Crommie, C.P. Lutz, D.M. Eigler, Science **262**, 218 (1993)
34. B.N.J. Persson, Surf. Sci. **258**, 451 (1991)
35. A. Milchev, J. Chem. Phys **78**, 1994 (1983); Electrochem. Acta **28**, 941 (1983); A. Milchev, M. Paunov, Surface Sci. **108**, 25 (1981)
36. N.C. Bartelt, T.L. Einstein, E.D. Williams, J. Vac. Sci. Technol. A **2**, 1006 (1984)
37. M.N. Barber, J. Phys. A **15**, 915 (1982)
38. T.T. Tsong, R. Casanova. Phys. Rev. Lett. **47**, 113 (1981); T.T. Tsong, Mat. Sci. Eng. A **353**, 1 (2003)
39. F. Watanabe, G. Ehrlich, J. Chem. Phys. **96**, 3191 (1992)
40. R.B. Griffiths, comment during discussion, Conference on Phase Transitions on Surfaces, Orono, ME, Aug. 1981.
41. R. Najafabadi, D.J. Srolovitz, Surf. Sci. **317**, 221 (1994) (Cf., for steps)
42. T.J. Stasevich, T.L. Einstein, S. Stolbov, Phys. Rev. B **73**, 115426 (2006)
43. T. Mueller, G. Ceder, Phys. Rev. B **80**, 024103 (2009), use cross validation in the context of a Bayesian approach to cluster expansions
44. R. Sathiyarayanan, T.L. Einstein, Surface Sci. **603**, 2387 (2009)
45. J. Shao, J. Am. Stat. Assoc. **88**, 486 (1993)
46. H.S. Johnston, C.A. Parr, J. Am. Chem. Soc. **85**, 2544 (1963); W.H. Weinberg, R.P. Merrill, Surface Sci. **33**, 493 (1972); C.Q. Sun, B.K. Tay, X.T. Zeng, S. Li, T.P. Chen, J. Zhou, H.L. Bai, E.Y. Jiang, J. Phys.: Condens. Matter **14**, 7781 (2002)
47. H.-C. Jeong, E. D. Williams, Surf. Sci. Rept. **34**, 171 (1999)
48. T.J. Stasevich, T.L. Einstein, R.K.P. Zia, M. Giesen, H. Ibach, F. Szalma, Phys. Rev. B **70**, 245404 (2004)
49. T.J. Stasevich, H. Gebremariam, T.L. Einstein, M. Giesen, C. Steimer, H. Ibach, Phys. Rev. B **71**, 245414 (2005)
50. H. Ibach, W. Schmickler, Phys. Rev. Lett. **91**, 016106 (2003) (This simple equivalency does not hold for stepped surfaces in an electrochemical system, where the electrode potential ϕ is fixed rather than the surface charge density conjugate to ϕ .)
51. C. Rottman, M. Wortis, Phys. Rev. B **24**, 6274 (1981)
52. J.E. Avron, H. van Beijeren, L.S. Schulman, R.K.P. Zia, J. Phys. A **15**, L81 (1982); R.K.P. Zia, J.E. Avron, Phys. Rev. B **25**, 2042 (1982)
53. J.W. Cahn, R. Kikuchi, J. Phys. Chem. Solids **20**, 94 (1961)
54. S. Dieluweit, H. Ibach, M. Giesen, T. L. Einstein, Phys. Rev. B **67**, 121410(R) (2003)
55. N. Akutsu, Y. Akutsu, Surf. Sci. **376**, 92 (1997)
56. R. Van Moere, H.J.W. Zandvliet, B. Poelsema, Phys. Rev. B **67**, 193407 (2003)
57. H.J.W. Zandvliet, R. Van Moere, B. Poelsema, Phys. Rev. B **68**, 073404 (2003)
58. R.C. Nelson, T.L. Einstein, S.V. Khare, P.J. Rous, Surf. Sci. **295**, 462 (1993)
59. M. Giesen-Seibert, H. Ibach, Surf. Sci. **316**, 205 (1994); M. Giesen-Seibert, F. Schmitz, R. Jentjens, H. Ibach, Surf. Sci. **329**, 47 (1995)
60. T.J. Stasevich, T.L. Einstein, R.K.P. Zia, M. Giesen, H. Ibach, F. Szalma, Phys. Rev. B **70**, 245404 (2004)
61. Universal Connector Toy, United States Patent 6179681, now marketed by Superstructs. <http://www.wikipatents.com/US-Patent-6179681/universal-connector-toy> or <http://www.freepatentsonline.com/6179681.html>, 7 Sept, 2009
62. K. Berland, T.L. Einstein, P. Hyldgaard, Phys. Rev. B **80**, 155431 (2009)
63. D.B. Dougherty, P. Maksymovych, J. Lee, J.T. Yates, Jr., Phys. Rev. Lett. **97**, 236806 (2006)
64. G. Pawin, K.L. Wong, K.Y. Kwon, L. Bartels, Science **313**, 961 (2006)